Systems/Circuits

Emotional Memory Processing during REM Sleep with Implications for Post-Traumatic Stress Disorder

Young-Ah Rho,1 Jason Sherfey,2,3 and Sujith Vijayan1

¹School of Neuroscience, Virginia Tech, Blacksburg, Virginia 24061, ²Picower Institute for Learning and Memory, Massachusetts Institute of Technology, Cambridge, Massachusetts 02139, and ³Department of Psychological and Brain Sciences, Boston University, Boston, Massachusetts 02215

REM sleep is important for the processing of emotional memories, including fear memories. Rhythmic interactions, especially in the theta band, between the medial prefrontal cortex (mPFC) and limbic structures are thought to play an important role, but the ways in which memory processing occurs at a mechanistic and circuits level are largely unknown. To investigate how rhythmic interactions lead to fear extinction during REM sleep, we used a biophysically based model that included the infra-limbic cortex (IL), a part of the mPFC with a critical role in suppressing fear memories. Theta frequency (4–12 Hz) inputs to a given cell assembly in IL, representing an emotional memory, resulted in the strengthening of connections from the IL to the amygdala and the weakening of connections from the amygdala to the IL, resulting in the suppression of the activity of fear expression cells for the associated memory. Lower frequency (4 Hz) theta inputs effected these changes over a wider range of input strengths. In contrast, inputs at other frequencies were ineffective at causing these synaptic changes and did not suppress fear memories. Under post-traumatic stress disorder (PTSD) REM sleep conditions, rhythmic activity dissipated, and 4 Hz theta inputs to IL were ineffective, but higher-frequency (10 Hz) theta inputs to IL induced changes similar to those seen with 4 Hz inputs under normal REM sleep conditions, resulting in the suppression of fear expression cells. These results suggest why PTSD patients may repeatedly experience the same emotionally charged dreams and suggest potential neuromodulatory therapies for the amelioration of PTSD symptoms.

Key words: computational model; memory; oscillations; REM sleep

Significance Statement

Rhythmic interactions in the theta band between the mPFC and limbic structures are thought to play an important role in processing emotional memories, including fear memories, during REM sleep. The infralimbic cortex (IL) in the mPFC is thought to play a critical role in suppressing fear memories. We show that theta inputs to the IL, unlike other frequency inputs, are effective in producing synaptic changes that suppress the activity of fear expression cells associated with a given memory. Under PTSD REM sleep conditions, lower-frequency (4 Hz) theta inputs to the IL do not suppress the activity of fear expression cells associated with the given memory but, surprisingly, 10 Hz inputs do. These results suggest potential neuromodulatory therapies for PTSD.

Introduction

Sleep is thought to play an important role in processing and consolidating memories, including emotional memories (Wagner et al., 2006; Payne et al., 2008; Baran et al., 2012; Rasch and Born,

Received May 26, 2022; revised Nov. 15, 2022; accepted Nov. 22, 2022.

Author contributions: Y.-A.R. and S.V. designed research; Y.-A.R. and S.V. performed research; Y.-A.R., S.V., and J.S. contributed unpublished reagents/analytic tools; Y.-A.R. and S.V. analyzed data; Y.-A.R. and S.V. wrote the paper.

S.V. and Y.-A.R. were supported by U.S. Army Research Office Grant ARO W911NF-17-1-0300. S.V. also acknowledges support from Grant 2047529 from the United States National Science Foundation and Grant R21MH127567 from the National Institutes of Health.

The authors declare no competing financial interests.

Correspondence should be addressed to Sujith Vijayan at neuron99@vt.edu or Young-Ah Rho at yarho75@vt.edu.

https://doi.org/10.1523/JNEUROSCI.1020-22.2022 Copyright © 2023 the authors

2013). Both animal studies and human studies have implicated rapid eye movement (REM) sleep, the stage of sleep in which vivid dreams occur, in the processing of emotional memories (Wagner et al., 2001; Nishida et al., 2009; Popa et al., 2010; Datta and O'Malley, 2013), although there is evidence that other sleep stages may also be important (Cairney et al., 2015; Payne et al., 2015). Studies indicate the importance of theta band (4–12 Hz) activity in general and of interactions in the theta band between the prefrontal cortex and limbic structures during REM sleep for the processing of emotional memories (Nishida et al., 2009; Popa et al., 2010; Boyce et al., 2016; Kim et al., 2020).

However, the ways in which rhythmic interactions during REM sleep transform emotional memories at a mechanistic and circuits level are largely unknown. One important consideration is the fact that although local field potential (LFP) and EEG patterns look similar during awake periods and during REM sleep,

they arise under different physiological conditions. Serotonin and norepinephrine levels, for example, are much lower during REM sleep than during the awake state (Rasch and Born, 2013). The special physiological state of the prefrontal cortex, amygdala, and hippocampus during REM sleep may provide conditions that allow for the induction of neural connectivity changes that lead to the processing and consolidation of emotional memories.

Here, we employ biophysically based mathematical models that capture circuit-level dynamics to gain insight into how REM sleep processes emotional memories via rhythmic interactions between the prefrontal cortex and limbic structures. In particular, we examine the role of REM sleep in the extinction of fear memories (Datta and O'Malley, 2013). To this end, we focus on how the physiological conditions of REM sleep, in conjunction with rhythmic activity, impact the connectivity between the amygdala and the infralimbic portion of the medial prefrontal cortex, which is thought to play a central role in the extinction of fear memories (Sotres-Bayon and Quirk, 2010; Duvarci and Pare, 2014).

In addition, we hypothesized that aberrations in the circuit responsible for REM sleep-related extinction of fearful memories could lead to the symptomology of post-traumatic stress disorder (PTSD). PTSD patients often experience the same emotionally charged, fearful dreams over and over again (Spoormaker and Montgomery, 2008), and there is evidence that norepinephrine levels do not go down during REM sleep in PTSD patients (Mellman et al., 1995), unlike in the general population. We use our model to gain a better understanding of PTSD by examining the impact of high levels of norepinephrine during REM sleep on neural dynamics, the interactions between the prefrontal cortex and the amygdala, and plasticity and the processing of emotional memories.

We show that during REM sleep, 4 Hz inputs to a given cell assembly in the infralimbic cortex (IL), representing a given emotional memory, produce changes in network connectivity strengths that result in a reduction in the activity of fear expression cells associated with the memory. Higher frequencies in the theta band (e.g., 10 Hz) can produce similar changes, but lower-frequency (4 Hz) theta inputs are effective in producing such changes over a wider range of input strengths and, specifically, at lower input strengths. Inputs in other frequency bands are ineffective in producing these changes and suppressing the activity of fear expression cells. Under PTSD REM sleep conditions, 4 Hz inputs to IL also fail to reduce the activity of fear expression cells associated with a given memory. The ineffectiveness of inputs that normally suppress the activity of fear expression cells associated with a given memory may be why PTSD patients experience the same emotionally charged dream repeatedly. Surprisingly, under PTSD REM sleep conditions, higher-frequency (10 Hz) theta inputs are effective in bringing about changes in synaptic strengths that result in the suppression of the activity of fear expression cells associated with a given memory.

We note that throughout the manuscript when we refer to activation of a memory in the context of our model, we are referring to the activation of a given cell assembly, that is, an increase in the activity of the cells of the assembly. More explicitly, in the model we designate particular cell assemblies as being associated with particular memories in the sense that a cell assembly is active when the corresponding memory is expressed and that, in fact, activity in the cell assembly underpins the expression of the memory. This understanding of memory is based on research indicating that activation of particular cell assemblies is associated

with memory reactivation (Sakurai et al., 2018), along with the assumption that memory, as it is commonly understood as perception and measured via behavioral indicators, depends on this memory-specific activation of specific cell assemblies.

Materials and Methods

Single-cell models

We used conductance-based models governed by Hodgkin–Huxley-type equations to construct principal cells and interneurons in the amygdala and pyramidal neurons and interneurons in the medial prefrontal cortex (mPFC).

All our model cells have both somatic and dendritic compartments except for the interneurons in the mPFC, which are single-compartment models. The synaptic currents for the mPFC were modeled as described in Durstewitz et al. (2000), Durstewitz and Seamans (2002), and Sherfey et al. (2018b), and those for the amygdala as described in Li et al. (2009).

Our single-cell models incorporating both somatic and dendritic compartments were governed by the following equations:

$$\frac{C_s dV_s}{dt} = -g_{Ls}(V_s - E_{Ls}) - g_c(V_s - V_d) - \sum I_s^{int} - \sum I_s^{syn} + I_s$$

$$\frac{C_d dV_d}{dt} = -g_{Ld}(V_d - E_{Ld}) - g_c(V_d - V_s) - \sum I_d^{int} - \sum I_d^{syn} + I_d,$$

where V_s and V_d are the somatic and dendritic membrane potentials, respectively, and C_s and C_d are the specific membrane capacitances of the soma and the dendrite, respectively. I_s^{imt} , I_s^{sym} , and I_s (I_d^{imt} , I_d^{sym} , and I_d) are the intrinsic conductance, synaptic conductance, and applied current in the soma (dendrite), respectively, and g_c is the coupling conductance between the soma and the dendrite.

Amygdala. The basal nucleus (BA), along with the lateral nucleus (LA), is a part of the basolateral amygdala (BLA). The composition of the BA is $\sim\!80\%$ excitatory cells and 20% inhibitory cells (Washburn and Moises, 1992; Faber et al., 2001). Our BA principal cell models have two compartments representing the soma (diameter 15 μ m, length 15 μ m) and an apical dendrite (diameter 5 μ m, length 400 μ m).

All compartments in our model cells are modeled via point models. We list the compartment dimensions as they are needed to calculate certain point model parameter values from values given in the cited work, for example, to calculate calcium dynamics in the dendrite. Both somatic and dendritic compartments include a sodium current (I_{Na}), a potassium delayed rectifier current (IDR), a slow potassium current (IM), a highvoltage activated calcium current (I_{Ca}), and a leak current (I_L). Dendritic compartments contain the following additional currents: a hyperpolarization activated cation current (I_H), a potassium current that inactivates slowly (I_D), a C-type potassium current (I_C), and an afterhyperpolarization current that is not voltage sensitive and not sensitive to apamin (I_{sAHP}). The gating variables for all the ionic conductances were taken from Li et al. (2009). Principal neurons in the BA differ in their firing patterns in response to prolonged current injections, ranging from full-spike adaptation to firing repetitively because of the differential expression of voltage- and Ca²⁺-dependent K⁺ conductances. To capture the different firing properties of type-A cells, which display full adaptation, and type-C cells, which display relatively little adaptation, the conductance values of I_M, I_D, and I_{sAHP} were adjusted appropriately, in accordance with Li et al. (2009). In particular, the ionic conductances for A-type pyramidal neurons during REM conditions are as follows (densities given in mS/cm²): I_{Na} [S (soma), 120; D (dendrite), 40], I_{DR} (S, 12; D, 3), I_M (S, 0.3; D, 0.3), I_{Ca} (S, 0.1; D, 0.2), I_L (S, 0.034; D, 0.034), I_H (D, 0.1), I_D (D, 1), I_C (D, 0.5), I_{sAHP} (D, 0.1). The ionic conductances for C-type pyramidal neurons (in mS/cm²) are the following: I_{Na} (S, 120; D, 40), I_{DR} (S, 12; D, 3), I_{M} (S, 0.25; D, 0.25), I_{Ca} (S, 0.1; D, 0.2), I_{L} (S, 0.034; D, 0.034), I_{H} (D, 0.1), I_{D} (D, 0.1), I_{C} (D, 0.5), I_{sAHP} (D, 0.5). The membrane capacitance and reversal potential

for the leak current are $C_m=1.0~\mu F/cm^2$ and $E_L=-75~mV$, respectively. The above are the conductances under REM conditions; below, we detail how we move in our model from the healthy REM state to other states. The interneuron model also has two compartments representing a soma (diameter, $15~\mu m$; length, $15~\mu m$) and dendrite (diameter, $10~\mu m$; length, $15~\mu m$), with each compartment consisting of I_{Na} and I_{DR} currents. The ionic conductances for the interneurons (in mS/cm²) are as follows: I_{Na} (S, 35; D, 10), I_{DR} (S, 8; D, 3). For the interneuron model, $C_m=1.0~\mu F/cm^2$ and $E_L=-70~mV$.

mPFC. Two subregions, the prelimbic (PL) cortex and the IL cortex within the mPFC, are thought to play distinct roles in fear learning. In particular, it is thought that PL activation facilitates the expression of conditioned fear, whereas IL activation facilitates the extinction of fear expression. Based on models by Durstewitz et al. (2000) and Durstewitz and Seamans (2002), we constructed both PL and IL pyramidal cells, each of which have two compartments (Durstewitz and Gabriel, 2007; Sherfey et al., 2018b) representing a soma (diameter, 21.84 µm; length, 28.618 μm) and an apical dendrite (diameter, 6.5 μm; length, 650 μm). Both the soma and the dendrite consist of an $\rm I_{Na}, I_{DR}, I_{C},$ a persistent sodium current (I_{NaP}), a potassium current that is slowly inactivating (I_{KS}), and a high-voltage-activated calcium current (I_{HVA}). The interneurons have one compartment with $I_{\rm Na}$ and $I_{\rm DR}$ currents. IL neurons within L2/ 3 have been shown to be more excitable than those in PL, possibly because of a lower spike threshold and higher input resistance in IL neurons (Song and Moyer, 2018). To reproduce the differing intrinsic excitability of cells in IL and PL, the leak conductance density (gleak) was adjusted so that g_{leak} was scaled down by 20% for PL and by 50% for IL pyramidal neurons from the original values taken from Durstewitz et al. (2000) and Durstewitz and Seamans (2002). In particular, the ionic conductances for our IL pyramidal neurons under REM conditions are as follows (densities in mS/cm²): I_{Na} (S, 117; D, 20), I_{DR} (S, 50; D, 14), I_{Nap} $(S,\,1.8;\,D,\,0.8),\,I_{KS}\,(S,\,0.08;\,D,\,0.08),\,I_{leak}\,(S,\,0.05;\,D,\,0.096),\,I_{HVA}\,(S,\,0.4;\,0.096)$ D, 0.8), $I_{\rm C}$ (S, 2.6; D, 2.1). The membrane capacitances for IL pyramidal neurons are (in $\mu F/cm^2$): C_m (S, 1.2; D, 2.304). The ionic conductances for PL pyramidal neurons are as follows (densities in mS/cm²): I_{Na} (S, 117; D, 20), I_{DR} (S, 50; D, 14), I_{Nap} (S, 1.8; D, 0.8), I_{KS} (S, 0.08; D, 0.08), I_{leak} (S, 0.08; D, 0.1536), I_{HVA} (S, 0.4; D, 0.8), I_{C} (S, 2.6; D, 2.1). The membrane capacitances for PL pyramidal neurons are the following: C_{m} (the membrane capacitance in μ F/cm²; S, 1.2; D, 2.304). The ionic conductances for IL and PL interneurons are the same as follows (densities in mS/cm²): I_{Na} (S, 135), I_{DR} (S, 50), I_H (S, 0.01), I_{leak} (S, 0.125). The membrane capacitances for IL and PL interneurons are the same, C_m (1.2 μ F/cm²). The mPFC principal cells and interneurons have E_L = -70and $-72 \,\mathrm{mV}$, respectively.

We consider only the superficial layers (L2/3) in our network model because we are not aware of any evidence suggesting the existence of connectivity from the deep layers to the superficial layers of IL or PL, and the BA region does not receive any inputs directly from the deep layers of PL or IL.

Network structure and synaptic currents

Network structure. We built a network model consisting of PL, IL, and BA components. In our model there are 120 excitatory neurons (24 in PL, 24 in IL, 48 A type and 24 C type in BA), and 40 inhibitory neurons (4 in PL, 4 in IL, 32 in BA). Each subregion (i.e., PL, IL, and BA) consists of cell assemblies embedded in a network. PL and IL have two assemblies of excitatory pyramidal neurons and associated inhibitory interneurons, and BA has four assemblies of excitatory principal neurons and associated inhibitory interneurons. In PL and IL, each assembly of excitatory neurons contains 12 pyramidal neurons (PY), and assemblies in both IL and PL receive inputs from four interneurons. In BA, each assembly of excitatory neurons consists of 12 A-type and six C-type cells, and eight interneurons.

Note that we are using the term "cell assembly" to refer to a group of cells that are strongly interconnected with one another. We assign each cell assembly a role in encoding a memory. For example, cell assembly BA1 in the BA represents a particular fear memory, BA3 represents the fear suppression cells associated with that fear memory, and cell assemblies PL1 and IL1, in the PL and IL, respectively, are associated with the

same fear memory through connections with BA1 and BA3. We are modeling not the initial encoding of the memory but the dynamics of cell ensembles after the memory has already been encoded during awake behavior. What the connectivity density in such a cell assembly would be *in vivo* is not clear. The connectivity probability of neurons in our network is set to be 100% (all-to-all connectivity) within assemblies and between certain assemblies representing the same memory (e.g., IL1 and BA3; Fig. 1A), and 10% between all other assemblies. We explored lower connectivity probabilities but found that the results were qualitatively the same. Specifically, when the connectivity probability was reduced from 100 by 50 or by 75%, the plastic changes that occurred in response to external rhythmic inputs were qualitatively the same as those seen with connectivity as described above.

In addition, all PY cells in PL and IL are reciprocally connected with fast-spiking interneurons (FS) in an all-to-all fashion. In BA, each assembly of excitatory neurons (12 A-type and six C-type cells) is connected to two subpopulations of interneurons, and the two subpopulations of interneurons are reciprocally connected to one another. One subpopulation is reciprocally connected to the excitatory cells, whereas the other has one-way projections to the excitatory cells (Fig. 1*A*).

Our model incorporates connections between subregions based on experimental findings. BA inputs are known to project directly into L2/3 in PL and IL, targeting the dendritic spines of pyramidal neurons, suggesting direct feedforward excitation of cells (Bacon et al., 1996), and the target pyramidal cells of L2/3 in PL and IL project back to the BA (Ghashghaei and Barbas, 2002; Ghashghaei et al., 2007; Onge et al., 2012; Little and Carter, 2013; Yizhar and Klavir, 2018; Fig. 1A). We incorporate two putative connections suggested by Duvarci and Pare (2014) based on the amygdala literature, a direct connection from pyramidal cells in IL onto interneurons in the BA and a connection from fear extinction cells in the BA onto interneurons that project to fear neurons in the BA (Fig. 1A, orange connections).

Synaptic interactions and spike-timing-dependent plasticity. All the neurons in our network model are connected either via excitatory AMPA and NMDA connections or inhibitory GABA connections. The synaptic current equations and parameters for BA were taken from Li et al. (2009), and those for mPFC were taken from Durstewitz et al. (2000) and Sherfey et al. (2018b). Both AMPA and NMDA receptors were simulated on the dendritic compartments in BA and mPFC, and GABA receptors were simulated on the soma compartments in BA and mPFC, except for the interneurons in the mPFC, which were single-compartment models. For principal cells in the BA, the rise and decay times for AMPA receptors are 0.5 ms and 7 ms, respectively. For interneurons in the BA, the rise and decay times for AMPA receptors are 0.3 ms and 2.4 ms, respectively. In the BA, the rise and decay times for NMDA receptors are 5 ms and 125 ms, respectively, whereas the rise and decay times for GABA receptors are 0.25 ms and 3.75 ms, respectively. In the PFC, the rise and decay times for AMPA receptors are 0.2 ms and 1 ms, respectively. In the PFC, the rise and decay times for NMDA receptors are 2.3 ms and 95 ms, respectively, and the rise rise and decay times for GABA receptors are 0.5 ms and 5 ms, respectively.

To investigate the extinction of fear memories via changes in synaptic strength, we implemented spike-timing-dependent plasticity (STDP) mechanisms, which depend on the relative timing of presynaptic and postsynaptic spiking events (Bi and Poo, 1998; Gerstner and Kistler, 2002; Gütig et al., 2003; Pfister and Gerstner, 2006). In particular, we implemented an STDP mechanism that employs a triplet learning rule as described in Pfister and Gerstner (2006). Whereas most of the cells in our network model are connected via general synaptic connections as described above, the colored arrows in Figure 1A indicate synapses governed by STDP mechanisms; these include reciprocal connections between excitatory cells in mPFC and excitatory cells in BA as well as a subset of the excitatory inputs onto inhibitory cells in BA.

Neuromodulator effects

Here, we describe the changes made to move from REM conditions to awake conditions and from REM conditions to REM conditions under PTSD. During both REM sleep and the awake state, acetylcholine levels are relatively high, but during the awake state, norepinephrine and

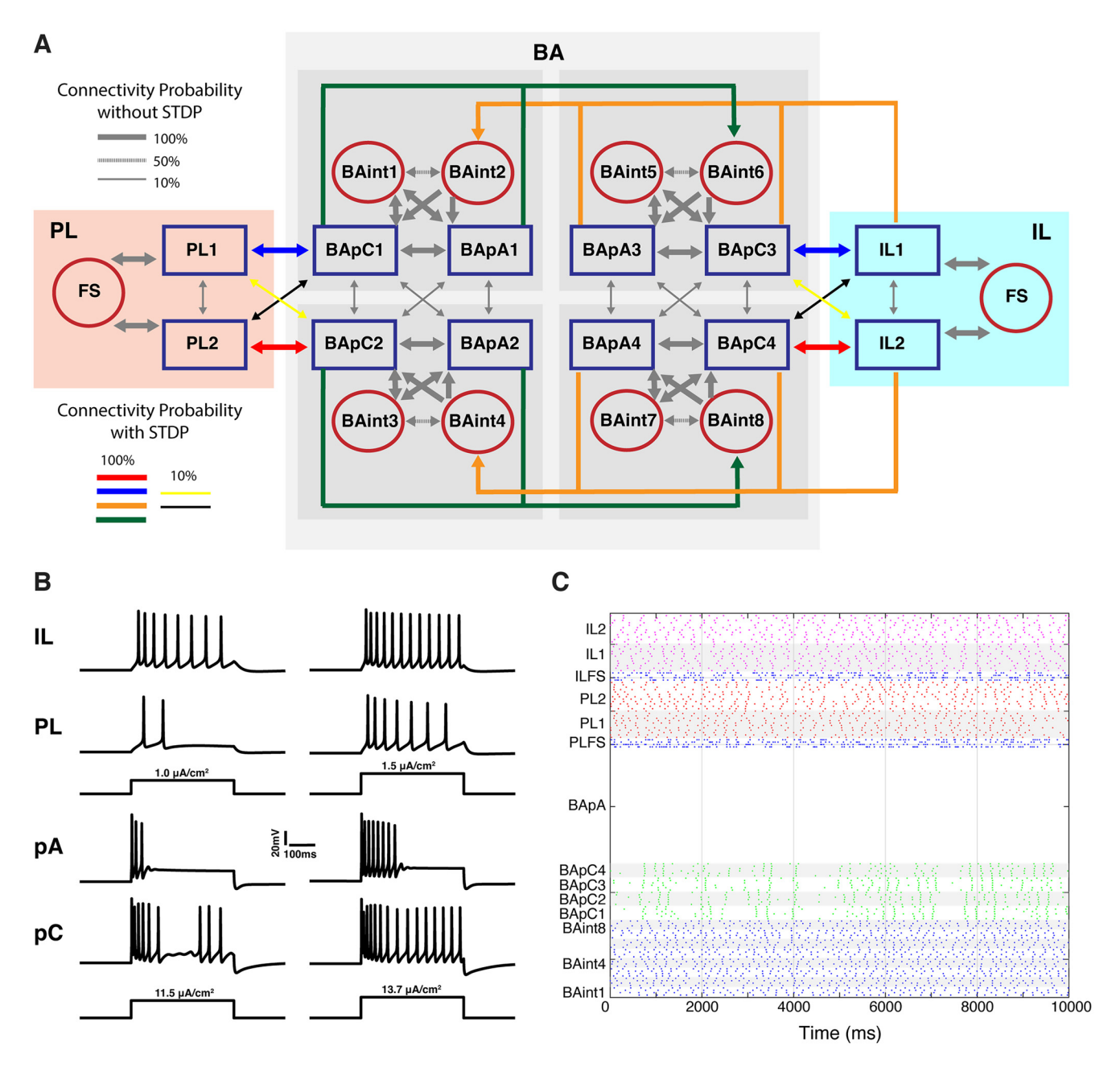


Figure 1. Network structure of BA-mPFC model, firing properties of model cells, and local network dynamics. *A*, Each subregion (PL, IL, BA) is composed of multiple cell assemblies. PL and IL each have two assemblies of excitatory pyramidal neurons and associated inhibitory neurons, and BA has four assemblies of excitatory principal neurons and associated inhibitory neurons. Cell assembly BA1 (consisting of BApC1, BApA1, and associated interneurons) and cell assembly BA2 (consisting of BApC2, BApA2, and associated interneurons) can be conceptualized as representing two distinct fear memories. BA3 (BA4) can be conceptualized as the assembly of fear suppression cells associated with the fear memory represented by BA1 (BA2). Shaded gray boxes demarcate cell assemblies. PL1 (PL2) is the cell assembly in the prelimbic cortex associated with the BA3 (BA4) fear suppression assembly. Colored arrows indicate synapses governed by STDP rules (see above, Materials and Methods, Network structure and synaptic currents), whereas gray arrows indicate synapses not governed by STDP rules. BApC, Principal cell type C of the BA; BApA, principal cell type A of the BA; BAint, interneurons of the BA; PL, pyramidal cells of the prelimbic cortex; IL, pyramidal cells of the infralimbic cortex; PLFS, fast spiking cells in PL; ILFS, fast spiking cells in IL. For connections without STDP mechanisms incorporated, thick grey lines indicate 100% connectivity while hashed lines indicate 50% connectivity and thin grey lines indicate 10% connectivity. *B*, Rows 1, 2, The voltage responses of PL and IL cells to two 500 ms step currents (left, 1.0 μA/cm²). Rows 3, 4, The voltage responses of BA A-type and C-type cells to two 500 ms step currents (left, 1.1.5 μA/cm²). C, Rastergram reflecting local circuit dynamics during REM sleep in the PL, IL, and BA when model subregions are not interconnected. In other words, the cells within each subregion were connected, but cells in different subregions (i.e., IL, PL, and BA) were not connected.

serotonin levels are higher relative to those during REM sleep. Therefore, we increased norepinephrine and serotonin levels to go from the REM state to the awake state. Note that the locations of the receptors for these neurotransmitters (e.g., the types of cells in which they are expressed and their densities within those cell types) and the receptor subtypes that are present vary by brain region, and therefore the changes they induce can be quite different in different regions (McCormick, 1992). In the BA and the

mPFC, we made the appropriate adjustments to go from REM to the awake state based primarily on the modeling work of Kim et al. (2013) and Pendyam et al. (2013), who modeled the amygdala and PL, and the experimental work of Johnson et al. (2011), Bocchio et al. (2015, 2016). In their methods, appendices, and supplemental material, Kim et al. (2013) and Pendyam et al. (2013) listed the appropriate conductance values for use in modeling both lower and higher levels of various

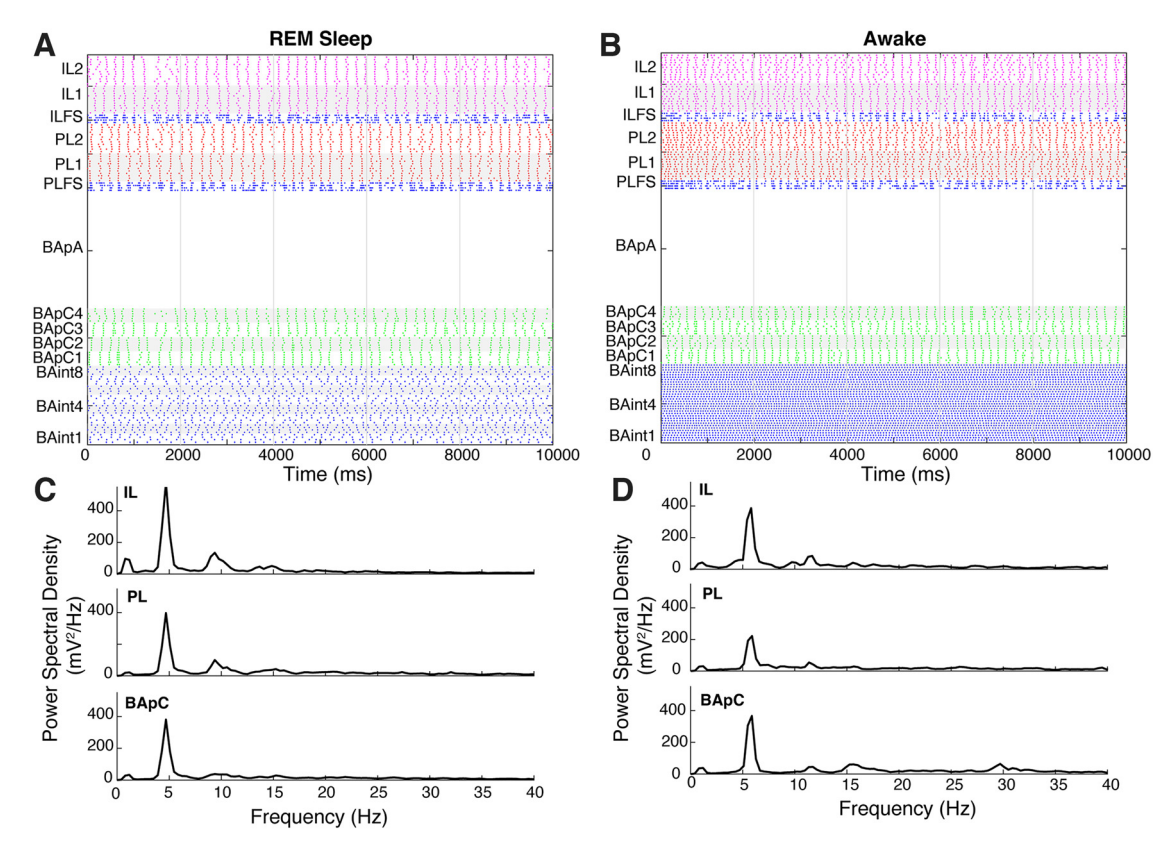


Figure 2. Spontaneous network activity during REM sleep and Awake conditions. **A**, Rastergram of neural network activity over the course of a 10 s simulation in the absence of external inputs during REM sleep conditions. **B**, Same as **A**, but during Awake conditions. **C**, The power spectral density during REM sleep in each subregion in our model. **D**, Same as **C**, but during Awake conditions.

neurotransmitters. To model awake conditions, we used the conductance values for higher levels of the relevant neurotransmitters. In particular, in BA principal cells, we decreased the potassium and sAHP conductances by 20%, and in BA interneurons, we decreased both the NMDA conductance and leak conductance by 20%. We modeled the net effect of increasing norepinephrine and serotonin in the mPFC as an increase in the excitability of the mPFC principal cells projecting to the amygdala, so we decreased the leak conductance by 5% in the pyramidal cells (Carr et al., 2007; Pendyam et al., 2013; Avesar et al., 2018).

To model PTSD REM conditions, we started with normal REM sleep conditions and increased the norepinephrine (NE) concentration to relatively high levels (Mellman et al., 1995). To implement high NE levels in the mPFC component of our model, we decreased the leak conductance by 2.5% and increased the NMDA conductance by 30% in the principal cells and interneurons, and increased the high-voltage-activated calcium conductance in the dendrites of principal cells by 2% (Barth et al., 2007; Carr et al., 2007; Ji et al., 2008; Pendyam et al., 2013). To implement high NE levels in the BA, we decreased potassium and sAHP conductances by 30%. In addition, NMDA conductances for principal cells receiving inputs from the PFC were increased by 33.33%, whereas NMDA conductances for interneurons receiving inputs from the PFC were decreased by 30% (Johnson et al., 2011; Kim et al., 2013; Pendyam et al., 2013).

Background input and external inputs used in simulations

We introduced background noise to our network model to mimic membrane potential fluctuations observed experimentally in neuronal systems. This noise is governed by the Ornstein-Uhlenbeck process (Uhlenbeck and Ornstein, 1930) as follows:

$$\frac{dI_{noise}}{dt} = \frac{I_{avg} - I_{noise}}{\tau_{noise}} + \sigma_{noise} N(0, 1),$$

where N(0,1) is a random number generated from a Gaussian distribution with mean zero and unit variance, where I_{avg} serves as a DC offset,

and there are noise amplitude (σ_{noise}) and filtering (τ_{noise}) terms; σ_{noise} was set to be 1.5 μ A/cm² and τ_{noise} was 5 ms. In conjunction with background noise, DC currents were set to match the spontaneous mean firing rates observed experimentally (Quirk et al., 1995; Burgos-Robles et al., 2009) in cell populations in each subregion. The mean firing rates given here were calculated for each individual model subregion (IL, PL, and BA) considered separately (i.e., not interconnected with other regions, in other words, under the condition that the cells within each subregion were connected but the cells in different subregions were not). Within the BA, the A-type cells do not fire (fire at 0 Hz) because of adaptive currents. BA C-type cells have an average firing rate of 2.6 Hz, which is within the range of experimentally reported firing rates for principal cells in the BA, 2-3 Hz (Herry et al., 2008). The BA interneurons fire at 4.0 Hz, which is within the range of reported spontaneous firing rates for BA interneurons, $2.81 \pm 0.52\,\mathrm{Hz}$ (Rosenkranz and Grace, 1999) and $\sim 6\,\mathrm{Hz}$ (Wolff et al., 2014, their Fig. 2D). The firing rates for the pyramidal cells in the PL and IL are 3.2 Hz and 3.0 Hz, respectively. These are close to the reported firing rates in PL and IL of 1-3 Hz (Jung et al., 1998). The firing rates for interneurons in the PL and IL are 7.9 Hz and 7.4 Hz, respectively, which are within the range of reported rates during REM and awake behavior, 5.59 \pm 7.25 Hz and 4.25 \pm 9.43 Hz, respectively (Watson et al., 2016).

External rhythmic inputs were simulated using a relatively peaked sinusoidal curve. These rhythmic inputs were applied directly to the dendritic compartments of cells and thus represent current injections. We used peaked sinusoidal inputs in the results presented here. We also examined how rhythmic synaptic inputs (modeled via AMPA channels) impact both the resonance properties of cells and the plasticity of their connections. With respect to resonance properties under REM sleep conditions, the results were similar to those seen using current injections (All cell types were able to fire at lower theta frequencies but not at other frequencies.), but on average a stronger synaptic input was needed to drive a given cell type. With respect to plasticity, the results

using synaptic inputs were qualitatively the same as those seen using sinusoidal current injections.

The frequency bands we considered were in the range of the major oscillations up to 80 Hz. In particular, we considered delta oscillations (0.5-4 Hz), theta oscillations (4-12 Hz), beta oscillations (15-30 Hz), and gamma oscillations (30-80 Hz). Note that there is no consensus on the exact number ranges for each oscillation, but relatively similar number ranges to the ones given above have been adapted across studies. These ranges also vary across species. In humans, theta oscillations are traditionally thought to occur at 4-8 Hz, and the alpha band encompasses 8-13 Hz oscillations. Within the theta band, we initially chose a specific frequency based on the resonance properties of the cells (4 Hz under healthy REM sleep conditions). Under PTSD REM sleep conditions, we noticed that the resonance properties of the cells changed; cells were more easily driven at 10 Hz under PTSD REM sleep conditions than under healthy REM sleep conditions. Because theta activity is thought to be especially important in limbic structures for processing emotional memories (Seidenbecher et al., 2003; Popa et al., 2010; Boyce et al., 2016), we therefore considered frequencies both in the lower range of theta (4 Hz) and in the higher range of theta (10 Hz).

The external step currents used to examine the impact of plasticity on fear memory suppression during awake conditions were also applied to the dendritic compartments of target neurons; these currents had a duration of 100 ms, were applied every 2 s, and had an amplitude of 6 μ A/cm² and 1 μ A/cm² in IL and BA, respectively.

Analysis and simulation methods

LFP and power spectrum. To determine the local field potential, all the dendritic membrane potentials of excitatory cells embedded in the same assembly were summed, and the summed voltages were normalized by subtracting the mean value of the summed voltages (Bazhenov et al., 2001; Hill and Tononi, 2005; Vijayan and Kopell, 2012). To calculate the power spectra for frequencies ranging from 1 to 40 Hz, the calculated LFPs were filtered using the MATLAB function bandpass, and then power spectral density was calculated using the MATLAB function pwelch. The power spectral density of the LFP in each subregion (i.e., IL, PL, or BA) was calculated by averaging across assemblies in the subregion.

Statistical analysis. We used a two-sample, unpaired t test to assess changes in the firing rates of cells before and after rhythmic external inputs during healthy REM sleep and during REM sleep under PTSD conditions. To account for multiple comparisons, we used Bonferroni corrections.

Numerics. Simulations were run in MATLAB using Dynasim, an open-source MATLAB toolbox for modeling neural networks (Sherfey et al., 2018a; http://dynasimtoolbox.org/). The differential equations were integrated using Euler's method with a time step of 0.01 ms.

Data availability

The model code is available at https://github.com/yarho75/REMCompModel.

Results

Single-neuron and local circuit dynamics in disconnected subregions during REM sleep

Before investigating the larger-scale circuit dynamics in the mPFC and amygdala, we examined the properties of individual neurons and local circuit dynamics in these areas.

We first verified that our single-neuron models exhibited the same firing patterns as those observed experimentally (Li et al., 2009; Pendyam et al., 2013; McGarry and Carter, 2017; Song and Moyer, 2018). As expected, the principal cells of the BA displayed various firing properties in response to prolonged stimulus inputs, with principal cell type A displaying relatively more adaption than principal cell type C. For instance, in response to a step current of 13.7 μ A/cm² for a duration of 500 ms, type-A cells initially fired eight spikes and then remained silent, whereas principal cell type C cells fired repetitively during the entire

stimulus (Fig. 1*B*). BA interneurons also displayed activity consistent with experimental results; they reproduced the experimentally observed repetitive firing patterns of fast-spiking cells. Also in line with experimental findings (Song and Moyer, 2018), given identical stimuli, mPFC cells in the infralimbic cortex (IL) were more excitable than those in the PL (Fig. 1*B*).

To examine local circuit dynamics during REM sleep in the prelimbic cortex, the infralimbic cortex, and BA, connectivity strengths for connections between BA and mPFC (IL and PL) were set to zero, whereas model cells within each subregion were connected as described (see above, Materials and Methods). DC currents in conjunction with background noise inputs to all cells were adjusted to match the spontaneous mean firing rates for each cell type as observed experimentally. Under these conditions, A-type cells were quiescent, and C-type cells showed periods of relative inactivity interspersed with periods of activity during which cells within assemblies burst in the theta frequency range (Fig. 1C, green dots). In addition, excitatory and inhibitory cells in the PL and IL fired irregularly without any clear spiking patterns.

Network activity during awake and REM sleep conditions

To examine network dynamics, we interconnected the mPFC and BA components (Fig. 1A; see above, Materials and Methods). Note that BA1 (consisting of BApC1, BApA1, and associated interneurons) and BA2 may be conceptualized as separate cell assemblies in BA representing two distinct fear memories. Similarly, BA3 and BA4 may be conceptualized as separate cell assemblies in BA representing fear extinction neurons for two distinct memories, with BA3 representing the fear extinction neurons for the memory represented by BA1 and BA4 representing the fear extinction neurons for the memory represented by BA2. PL1 and PL2 may be conceptualized as the cell assemblies in PL associated with BA1 and BA2, respectively, and IL1 and IL2 may be conceptualized as the cell assemblies in IL associated with BA3 and BA4, respectively.

We first explored spontaneous network activity in the absence of external inputs during both REM sleep and the awake state. Spike rastergrams under both REM sleep conditions and the awake state are depicted in Figure 2.

Surprisingly, under REM sleep conditions, all three of the subregions in our network exhibited theta activity. In BA, for instance (Fig. 2A), the excitatory neurons of assemblies 1 (BA1) and 2 (BA2), which are reciprocally connected to PL, spiked synchronously at the theta frequency (~5 Hz). Spiking in BA1 and BA2 was coherent with spiking in the excitatory cells of assemblies 1 (PL1) and 2 (PL2) in PL, which also showed pronounced rhythmic activity within the theta frequency range, ~5 Hz. The inhibitory neurons in BA also fired at ~5 Hz, although their firing was irregular and asynchronous. The excitatory neurons of assemblies 3 (BA3) and 4 (BA4) in BA, which are reciprocally connected to IL, fired synchronously with IL, analogous to the firing pattern observed in the PL-BA network. The inhibitory neurons of assemblies 2 (BAint2) and 4 (BAint4) in BA, which receive feedforward excitatory inputs from IL, exhibited higher firing rates than those of the other inhibitory neurons. The presence of theta activity was also seen at the level of the LFP in the BA, IL, and PL as evidenced by theta band peaks in the power spectra of the LFP (Fig. 2C; see above, Materials and Methods, for LFP calculations).

The rastergram in Figure 2B illustrates activity typical of the network during awake conditions. The excitatory neurons of BA1 and BA2, which are reciprocally connected to PL, exhibited

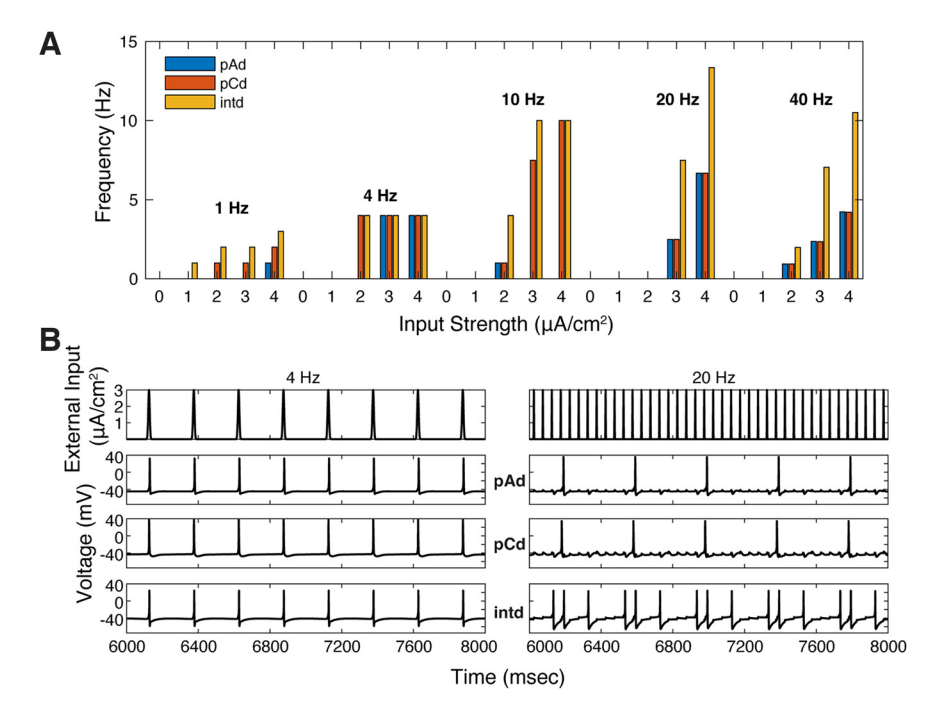


Figure 3. Cell-specific resonance properties in the BA under REM sleep conditions. **A**, Bar graph showing the mean firing rate of each cell type in the BA in response to external inputs with frequencies ranging from 1 to 40 Hz and input strengths varying between 1 and 4 μ LA/cm² (blue, A-type cell; red, C-type cell; yellow, interneuron). Here, a simplified network, consisting of three cells, one A type, one C type, and one interneuron, was used to examine the response properties of each cell type to external sinusoidal inputs. **B**, Depicted are the voltage traces of each cell type to 4 Hz (left) and 20 Hz (right) external inputs in the simplified network.

synchronous spiking patterns and fired at an average rate (\sim 6 Hz) a little higher than that seen during REM sleep conditions. The neurons in PL showed greater irregular activity than during REM sleep and fired at an average rate of \sim 7.3 Hz. The cells of BA3 and BA4, which are reciprocally connected to IL, also exhibited synchronous firing. The cells in IL fired more synchronously than those in PL, with an average firing rate of \sim 6.3 Hz. The inhibitory cells in BA fired at a higher rate (\sim 16 Hz) relative to that seen during REM conditions. The peak power in the LFPs tended to be higher in frequency and smaller in amplitude than that seen during REM conditions, especially in the PL and IL, likely because of there being a greater number of periods of asynchronous firing in both regions (Fig. 2D).

Cell-specific resonance properties

Because rhythmic activity is thought to be important for the processing of emotional memories, and as the source of such rhythmic activity may be brain areas not incorporated into our model, such as the hippocampus, we sought to examine the response properties of our model to different frequency external inputs. We first used a simplified network to examine the response properties of the amygdala cells to rhythmic inputs. In particular, we examined how varying the frequency of external inputs to amygdala cells affected their resonance properties when they were locally connected in a very simplified network consisting of one C-type principal neuron, one Atype principal neuron, and one interneuron. The frequencies of the external sinusoidal inputs to the cells were varied among 1, 4, 10, 20, and 40 Hz, and the input strengths were varied between 1 and 4 μ A/cm² (see above, Materials and Methods). We found that all cell types fired synchronously at the theta frequency when the external input frequency was in the lower

theta range (4 Hz), and the input strength was large enough, but that none of the cells could be entrained by beta or gamma frequency inputs, even for the strongest strength inputs (Fig. 3). Furthermore, the C-type cells and interneurons (but not the A-type cells) were able to fire at the lower theta frequency when given relatively weak inputs.

Changes in connectivity strength given different frequency external inputs during REM sleep

Because of differences in I_D, I_M, and I_{sAHP} currents, different cell types in the BA had differing propensities to respond to external inputs, resulting in differing resonance properties in the various cell types. We hypothesized that these differences might play a critical role in the plasticity mechanisms involved in the consolidation and extinction of emotional memories. To investigate how rhythmic activity and rhythmic inputs to the system might impact plasticity, we incorporated STDP mechanisms into our network; STDP mechanisms depend on the relative timing of presynaptic and postsynaptic spiking events (Gerstner and Kistler, 2002; Gütig et al., 2003; Pfister and Gerstner, 2006). STDP mechanisms

were incorporated at the connections between the mPFC and the amygdala and between the principal cells of the BA and the interneurons of the BA (Fig. 1A, colored arrows).

We first wanted to get a sense of how network activity impacted connectivity strengths in the absence of external inputs. Therefore, we examined the weight changes that occurred over a period of 200 s without external drive (Fig. 4A). The connections of cell assemblies that were sparsely interconnected (Fig. 4A, yellow and black traces) remained relatively unchanged in their weights. However, cell assemblies that spanned the mPFC and the BA and were connected in an all-to-all fashion (Fig. 4A, red and blue traces) experienced synaptic weight changes. In particular, cell assemblies involving BA to mPFC connections were potentiated over time (Fig. 4A, first and third row), indicating repeated spiking of cells in the BA before postsynaptic spiking of cells in the mPFC, whereas the synaptic weights for cell assemblies with mPFC to BA connections were depressed over time (Fig. 4A, second and fourth row), indicating repeated postspiking of cells in mPFC before prespiking of cells in BA. Of particular importance to the work here is that IL to BA connections for the highly connected cell assemblies were weakened, whereas BA to IL connections were strengthened.

The reciprocal nature of the change in the strength of mPFC-BA connections is likely because of the recurrent excitation involving these areas. Synaptic weights for connections where principal neurons synapsed onto interneurons in the BA increased slightly over time, suggesting that spiking of principal cells sometimes, but not always, preceded spiking of interneurons (Fig. 4B).

We wanted to examine how external inputs to the IL might impact connectivity between the IL and the BA cell assemblies

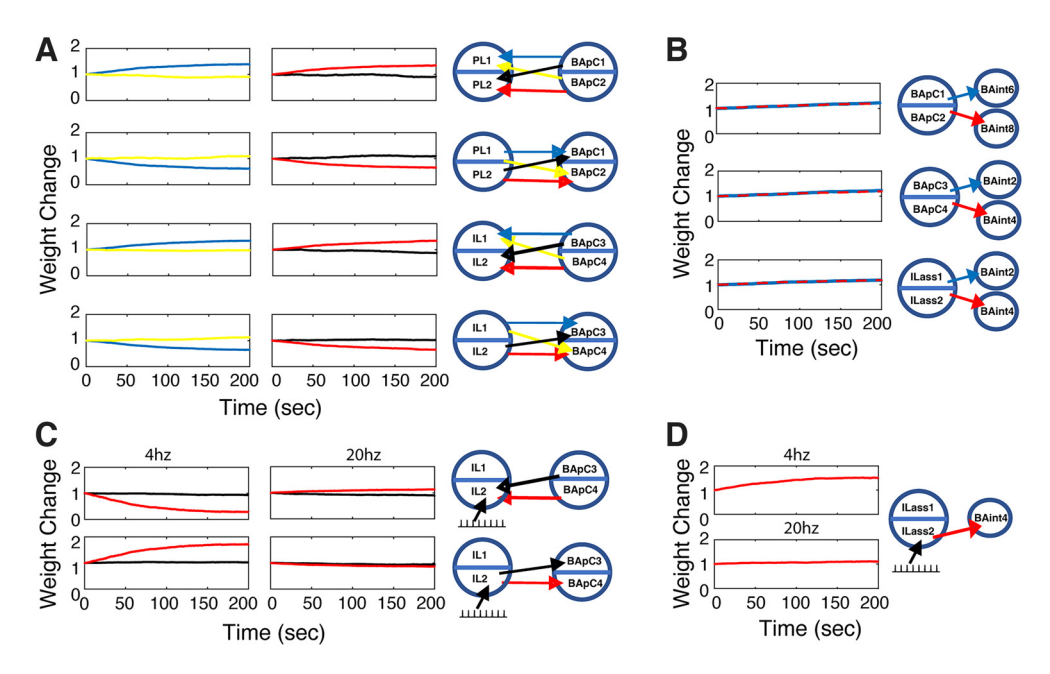


Figure 4. Changes in connectivity strength resulting from different frequency external inputs during REM sleep. **A**, Changes in the connectivity strength of connections between PL/IL neurons and BA excitatory neurons in the absence of external inputs over a period of 200 s. Right, Diagrams indicate which connections are depicted in the two columns (middle and left). For instance, the red line in the top row marks the average change in the synaptic strength of all the connections from BAPC2 to PL2. Note that the connectivity of sparsely connected cell assemblies was denoted by yellow and black lines, and the connectivity of cell assemblies that were connected in an all-to-all fashion were denoted by red and blue lines. **B**, Connectivity strength changes for connections from IL and BA excitatory neurons to BA inhibitory neurons in the absence of external inputs over a period of 200 s. **C**, Connectivity strength changes for connections between IL and BA in response to external rhythmic inputs (left, 4 Hz; right, 20 Hz) applied to IL2. The red line denotes all-to-all connectivity, and the black line denotes connectivity with 10% probability. **D**, Connectivity strength changes for connections from IL2 to BAint4 in response to external rhythmic inputs (top, 4 Hz; bottom, 20 Hz) applied to IL2.

and thus influence the processing of fear memories. In particular, we investigated how synaptic weights were affected by external rhythmic inputs, representing inputs from sources such as the hippocampus. The frequencies of external sinusoidal inputs applied directly to IL2 in IL were 1, 4, 20, and 40 Hz. Interestingly, we found that when a 4 Hz external input was introduced to IL2, the synaptic weights for BA4 to IL2 connections were remarkably depressed over time, whereas the weights in the opposite direction (for IL2 to BA4 connections) were largely potentiated (Fig. 4C, left column). Note that cell assemblies BA4 and IL2 are highly interconnected. In essence, the 4 Hz external drive to IL2 induced spiking in IL2 that preceded the spiking of BA4 cells, reversing the directionality of the change in connectivity strength seen in the absence of external inputs. The 4 Hz input also markedly increased the strength of the connections from IL2 to BAint4 (Fig. 1), that is, the BA interneurons that project to BA2 but lack reciprocal connections originating from BA2 (Fig. 4D, top row). Moreover, for external inputs at other frequency ranges, synaptic weight changes were not pronounced and had the same directionality as those in the absence of external inputs. For instance, given a 20 Hz input, the cells in IL2 did not follow the 20 Hz input; they fired ~ 8.5 times per second on average and in an irregular manner (Fig. 4C, right column; Fig. 4D, bottom row). Given this firing pattern, IL cells were not able to consistently produce spikes in BA neurons, which spiked in the theta range. Results were qualitatively similar at other frequencies.

Impact of weight changes during REM sleep on the extinction of fear memories

We examined how these synaptic weight changes, obtained via the interaction of STDP mechanisms with rhythmic activity during REM sleep, impacted the suppression of fear memories under awake conditions. In our model, there are two large subnetworks, one representing the fear memory circuit of PL and BA (BA1 and BA2), and the other representing the fear extinction circuit of IL and BA (BA3 and BA4). As mentioned previously, the cells in assemblies BA1 and BA2, and BA3 and BA4 can be conceptualized as representing fear memory cells and fear extinction cells, respectively. Furthermore, BA1 (BA2) and BA3 (BA4) represent the fear and extinction cells for the same memory. We found that the synapses from IL2 onto BAint4 and from BA4 onto BAint4 (Fig. 1A, orange lines) were potentiated during REM sleep in the presence of external theta inputs. These synaptic changes resulted in BAint4 receiving much stronger feedforward excitatory inputs than under baseline REM sleep conditions in our model.

We then sought to examine how these weight changes translated into the suppression of fear memories in the awake condition. To do this, we froze the synaptic weights at the values held at the conclusion of the REM simulation. Then, under awake conditions, we applied 56 step currents, each 100 ms in duration and at 2 s intervals, to IL2, BA2, and BA4; these three assemblies can be conceptualized as being associated with the same emotional memory. Note that the interneurons in BAint4 receive feedforward excitation from IL2 and BA4. We then calculated the mean firing rates of fear memory cells (BA2) during the 56 presentations of the step currents; note that BA2 receives feedforward inhibitory inputs directly from BAint4, and the BAint4 interneurons receive feedforward drive from the corresponding fear extinction cells (BA4), corresponding to the fear memory in BA2. The increased firing rates in the fear extinction cells (firing in response to the presentation of external step currents) relative to pre-REM sleep firing rates, along with an increase in the strength of the connections onto the interneurons in BAint4, resulted in an increased drive to the BAint4 interneurons and therefore significantly reduced spiking in the fear memory cells

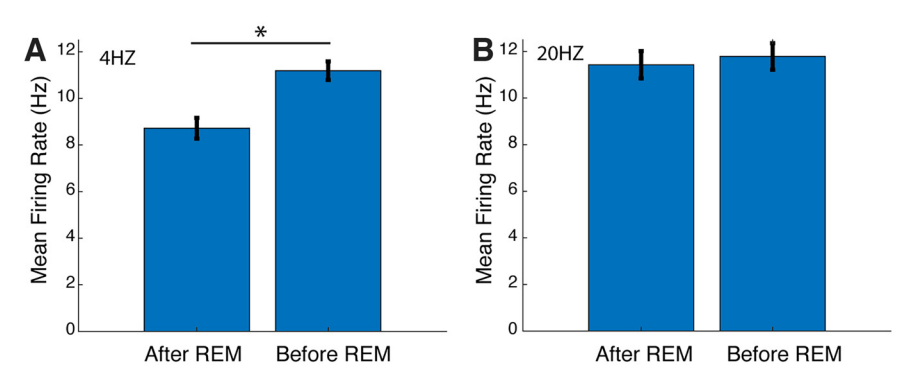


Figure 5. Impact of weight changes during REM sleep on the extinction of fear memories in the awake state. **A**, Average activity of fear expression cells in response to the application of step currents to components of the emotional memory network. After REM, synaptic weights are derived from the presentation of 4 Hz inputs to IL during REM sleep conditions. Before REM uses baseline synaptic weights (before any weight changes). **B**, Same as **A**, but for 20 Hz external inputs. Error bars indicate SEM; *p < 0.05 after Bonferroni correction.

in BA2 (p = 0.0000692, two-sample, unpaired t test, p < 0.05 after Bonferroni correction; Fig. 5A).

Next, to validate the importance of theta rhythmic interactions for the extinction of fear memories, we examined how weight changes induced by other frequency inputs during REM sleep impact the activity of fear expression cells during subsequent wake conditions. As the weight changes were similar for the nontheta frequencies, we decided to focus on one frequency, $20 \, \text{Hz}$. We presented the exact same sequence of step currents to the same assemblies as described above but using the synaptic weight values from the end of the REM simulation in which $20 \, \text{Hz}$ external inputs were presented to IL; we found that these synaptic weights, when introduced into the awake model, did not significantly reduce firing rates in fear memory cells (p = 0.66, two-sample, unpaired t test; Fig. 5B).

Network activity and cell-specific resonance properties of REM sleep under PTSD conditions

We next used our model to probe the neural dynamics of REM sleep in individuals with PTSD. There is evidence that unlike what is seen in the general population, norepinephrine levels do not go down during REM sleep (Mellman et al., 1995). Therefore, to mimic REM sleep in PTSD patients in our model, we started with the physiological conditions of REM sleep and made the appropriate adjustments to mimic high norepinephrine levels (see above, Materials and Methods). Under PTSD REM sleep conditions, the overall excitability of the cells in our model increased, and the theta rhythm in each subregion dissipated (Fig. 6A). In BA, A-type excitatory cells spiked rarely, although more than during healthy REM sleep conditions, likely because of the increased excitatory drive from mPFC neurons. C-type excitatory cells spiked at a higher firing rate but more irregularly than during healthy REM sleep conditions (~9 Hz) and exhibited intermittent periods of synchronous rhythmic activity like cells in the mPFC. In comparison with the LFP under healthy REM conditions, the LFP under PTSD REM conditions showed reduced power in the theta range in all regions of our model (Fig. 6B).

We next examined how PTSD REM sleep conditions might impact the resonance properties of cells in our model. As the cells in our network are more excitable under PTSD conditions, we hypothesized that they might be able to better follow relatively higher frequency inputs. As before, external sinusoidal inputs of different frequencies and input strengths were applied to a simple network but under PTSD conditions. Surprisingly,

we found that under PTSD conditions, like during healthy REM sleep, all cell types were able to synchronize with each other in the lower theta range (4 Hz). Similar to REM conditions, the cells in our network were not entrained by beta or gamma frequency inputs, even with relatively high input strengths. However, relatively strong inputs in the higher theta range (10 Hz) were able to entrain C-type cells and interneurons to 10 Hz and A-type cells to slightly <10 Hz (Fig. 7).

Changes in connectivity strengths because of different frequency external inputs under PTSD REM sleep conditions

We then sought to investigate how PTSD REM sleep conditions have impact synap-

tic weight changes in our model. First, we examined weight changes during PTSD REM sleep conditions in the absence of external inputs. For given cell assemblies in the mPFC and the BA with a low probability of connection between them, synaptic weights remained relatively unchanged. For given cell assemblies in the mPFC and the BA with a high probability of connection, the BA to mPFC connections were potentiated, whereas those from mPFC to BA were depotentiated. That is, the overall change in connectivity strength in interconnected assemblies located in the mPFC and the BA occurred in the same direction as that seen during normal REM sleep, although to a much lesser extent (Fig. 8A). Also, the synaptic weights for connections from BA principal neurons to BA interneurons increased slightly over time—once again, similar to what was seen during REM sleep under normal physiological conditions (Fig. 8B).

Next, we examined how external rhythmic inputs during PTSD REM sleep conditions changed the synaptic weights of connections between the mPFC and the BA. We found that during REM sleep under PTSD conditions, 4 Hz inputs to IL2 caused changes in synaptic weights to a lesser extent than during healthy REM sleep conditions (Fig. 8C, left column, D, top). However, interestingly, when external input frequencies at 10 Hz were introduced to IL2, synaptic weights for connections from IL2 to BA4 were prominently potentiated over time, whereas the weights for connections from BA4 to IL2 were remarkably depressed (Fig. 8C, right column). With 10 Hz inputs, the weights for connections from IL2 to BAint4 were also highly potentiated (Fig. 8D, bottom). We note that during healthy REM sleep conditions, 10 Hz inputs to IL2 potentiate connections from IL2 to BA4 while depotentiating connections from BA4 to IL2; however, the minimum strength of 10 Hz inputs needed to bring about such changes is greater than that for 4 Hz inputs.

Impact of weight changes during REM sleep on emotional memory expression during the awake state

Finally, we investigated how synaptic weight changes, gained through rhythmic interactions via STDP mechanisms during PTSD REM conditions, affected fear memory extinction during awake conditions. When using synaptic weights obtained using external 4 Hz inputs during PTSD REM sleep conditions, the firing rates in fear memory cells remained unchanged from the baseline awake condition (p = 0.4392, two-sample, unpaired t test; Fig. 9A). However, we found that introducing 10 Hz rhythmic external inputs to IL under PTSD conditions increased synaptic

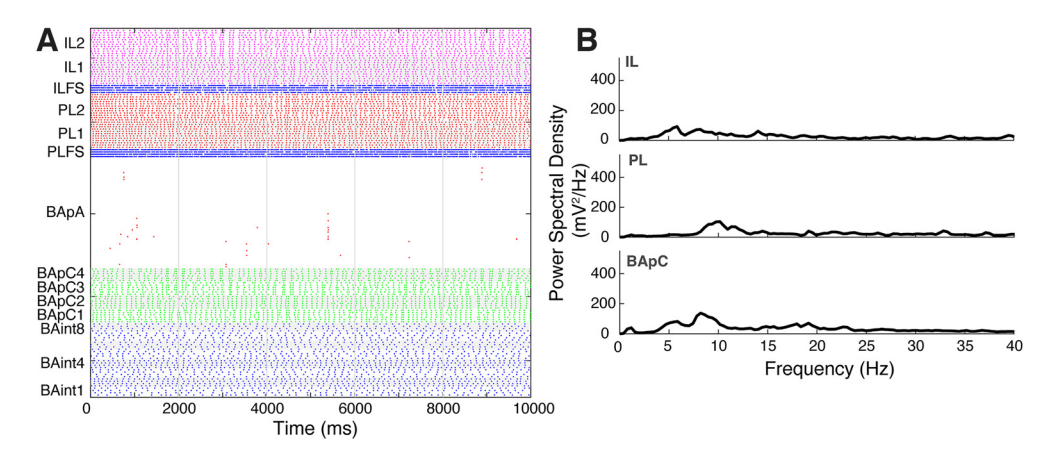


Figure 6. Spontaneous network activity during REM sleep under PTSD conditions. Same as Figure 2, A and B, but under PTSD REM conditions.

weights in a manner qualitatively similar to that seen when introducing 4 Hz inputs to IL during normal REM sleep conditions. Therefore, we considered the effect of using synaptic weights obtained through rhythmic interactions with 10 Hz inputs. Surprisingly, when using the synaptic weights obtained using 10 Hz external inputs under PTSD REM sleep conditions, our step current protocol resulted in increased firing rates in fear extinction cells, leading to reduced firing rates in fear memory cells (p = 0.0072, two-sample, unpaired t test, p < 0.05 after Bonferroni correction; Fig. 9B).

Discussion

We used a biophysically based network model to show that during REM sleep, theta frequency inputs (but not other frequency inputs) to a given cell assembly in IL bring forth changes in network connectivity strength that result in the suppression of the activity of fear expression cells for the associated memory, with lower theta frequency inputs (4 Hz) being effective over a wider range of input strengths.

Under PTSD REM sleep conditions, however, 4 Hz inputs to IL were ineffective in inducing these connectivity changes, whereas 10 Hz inputs were effective. These results suggest why PTSD patients might experience the same emotionally charged dreams repeatedly and suggest potential neuromodulatory therapies to ameliorate the symptoms of PTSD.

Fear memory suppression

Animal studies suggest that the IL (along with the amygdala, the hippocampus, and the connections among all three regions) is critical for fear extinction (Bouton et al., 2006; Pape and Pare, 2010; Sotres-Bayon and Quirk, 2010; Bloodgood et al., 2018). For example, the inactivation of IL can disrupt fear extinction, and the stimulation of IL can speed up fear extinction (Milad and Quirk, 2002; Sierra-Mercado et al., 2011). Furthermore, studies suggest that REM sleep and REM sleep-related dynamics are important for the processing and extinguishing of fear memories

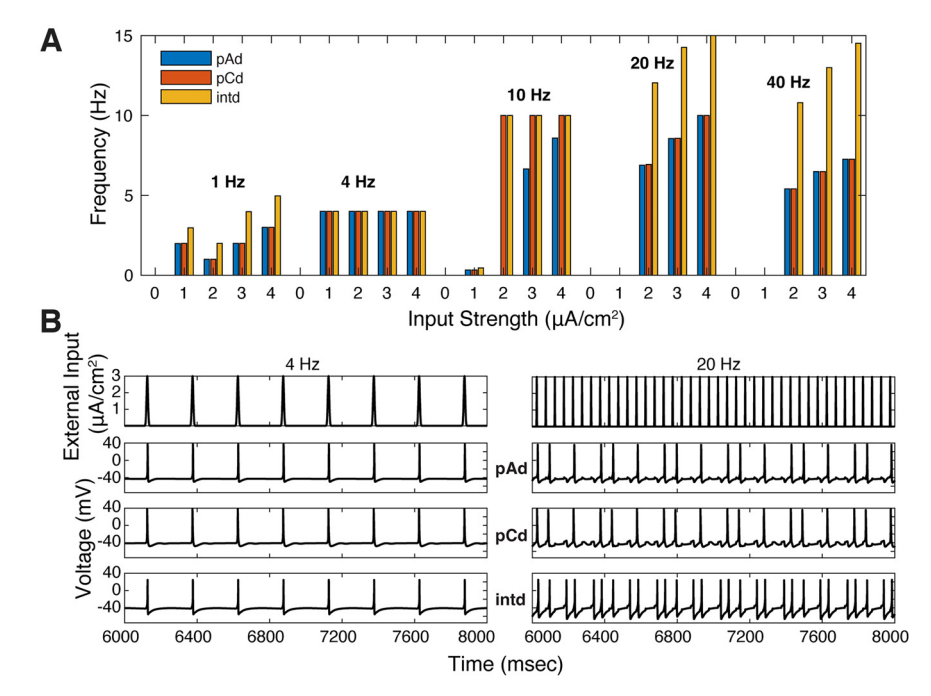


Figure 7. Cell-specific resonance properties under PTSD REM sleep conditions. Same as Figure 3, *A* and *B*, but under PTSD REM sleep conditions.

(Fu et al., 2007; Spoormaker et al., 2010; Datta and O'Malley, 2013; Pace-Schott et al., 2014).

Studies suggest that theta oscillations are of importance for emotional processing during REM sleep (Nishida et al., 2009; Popa et al., 2010; Boyce et al., 2016; Kim et al., 2020). Theta oscillations occur in the limbic and mPFC structures during REM sleep (Cantero et al., 2003; Nishida et al., 2009; Popa et al., 2010; Boyce et al., 2016; Vijayan et al., 2017), and their presence seems to be correlated with the consolidation of emotional memories (Popa et al., 2010), whereas their disruption can impair the processing of emotional memories (Boyce et al., 2016). Theta oscillations are coherent across limbic and mPFC structures during periods of REM sleep, and the directionality of theta communication is related to whether a given fear memory is strengthened or weakened (Popa et al., 2010).

Here, we examine how rhythmic activity, in particular theta oscillations, during REM sleep may support the suppression of fear memories. Under the physiological conditions of REM sleep, our model exhibited theta oscillations in all components—IL,

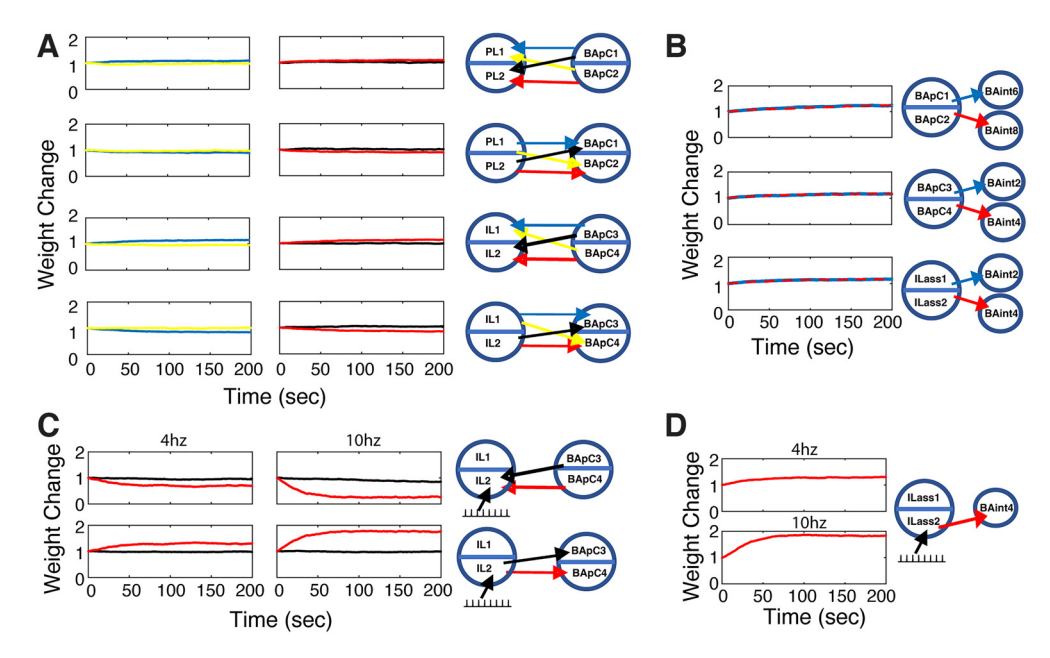


Figure 8. Changes in connectivity strength resulting from different frequency external inputs under PTSD REM sleep conditions. **A**, Same as Figure 4A, but for PTSD REM sleep conditions. **B**, Same as Figure 4B, but for PTSD REM sleep conditions with 4 Hz and 10 Hz external inputs to IL2. **D**, Same as Figure 4D, but for PTSD REM sleep conditions with 4 Hz and 10 Hz external inputs to IL2.

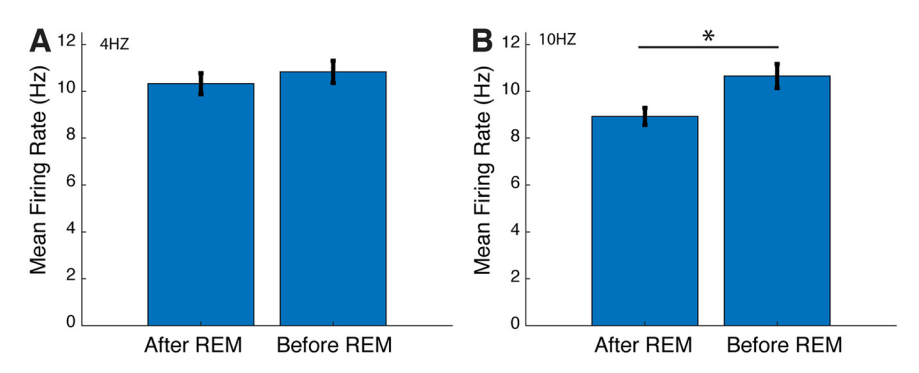


Figure 9. Impact of weight changes during PTSD REM sleep conditions on the extinction of fear memories in the awake state. **A**, Same as Figure 5A, but for 4 Hz inputs during PTSD REM sleep. **B**, Same as Figure 5A, but for 10 Hz inputs during PTSD REM sleep.

PL, and BA. We found that for a set of cell assemblies representing the same emotional memory in the various components of our model, connections from the amygdala to the IL were strengthened, whereas those from the IL to the amygdala were weakened during REM sleep with no external inputs to the IL-PL-BA system. In contrast, when IL received an external input of 4 Hz, connections from the amygdala to the IL were weakened, and those from the IL to the amygdala were strengthened. When other frequency band inputs were used (1, 20, and 40 Hz), the synaptic changes qualitatively resembled those in the freerunning condition (i.e., without external rhythmic inputs). Furthermore, connectivity changes that ensued from 4 Hz external inputs to just one of the cell assemblies in IL resulted in that assembly, along with the associated fear suppression cell assembly in BA, acting to reduce the activity of the corresponding fear expression cell assembly in BA.

These results suggest that 4 Hz inputs to IL during REM sleep, but not frequencies in other bands, have the ability to increase the drive from the IL to the amygdala while also decreasing the drive from the amygdala to the IL. It may be the case that if the brain deems a given context safe, the hippocampus might provide theta

band input to the appropriate cell assembly in the IL when the memory related to that context is processed during REM sleep, ultimately reducing the activity of the related fear cells in the BA. Our model thus predicts that REM-sleep-mediated fear extinction involves increased theta drive to the IL and that lower theta band inputs are most effective in doing this. Furthermore, our model predicts that whether a fear memory is suppressed may depend on whether IL receives external lower theta band drive during REM sleep.

In addition to the inhibition of fearexpressing neurons in the BA, theta inputs to the IL likely also lead to increased inhibition of the medial part of the central nu-

cleus (CeM) via the medial ventral portion of intercalated masses (ICMs; Duvarci and Pare, 2014). The central nucleus mediates many fear-related behavioral responses. The ICMs send inhibitory projections to the central nucleus and in turn receive input from the IL and the BA; there are direct excitatory projections from the IL to the ICMs and possibly also excitatory connections from fear extinction cells in the BA to the ICMs (Duvarci and Pare, 2014). Increased inhibition of the CeM could result from theta inputs to the IL potentiating direct excitatory inputs to the ICM and/or via increased drive from the fear suppression cells in the BA to the ICM; note that this latter possibility is supported by our model, which suggests that the theta rhythm increases the strength of connections from IL to the fear suppression cells in the BA.

Features not included in our model

As mentioned earlier, we consider only the superficial layers (L2/3) in our network model of IL and PL because we are not aware of any evidence suggesting the existence of connectivity from the deep layers to the superficial layers of IL or PL,

and the BA does not receive any inputs directly from the deep layers of PL or IL. BA neurons project directly into L2/3 in PL and IL, (Bacon et al., 1996), and the target pyramidal cells of L2/3 in PL and IL project back to the BA (Ghashghaei and Barbas, 2002; Ghashghaei et al., 2007; Onge et al., 2012; Little and Carter, 2013; Yizhar and Klavir, 2018). It is possible that connections do exist between the deep layers and superficial layers and have yet to be characterized; however, considering that they have yet to be identified, we would expect such connections to be relatively sparse. If such connections do exist, this could potentially have an impact on our findings.

Translation to human REM sleep and fear extinction

Experimental work in humans suggests that sleep, and REM sleep in particular, is important for the extinction of fearful memories (Spoormaker et al., 2010, 2012; Pace-Schott et al., 2012, 2014). Human studies suggest that during REM sleep, mPFC and limbic structures are highly active (Maquet et al., 1996; Nofzinger et al., 1997) and that theta activity is prominent in these structures; for instance, theta activity is present in the hippocampus (Cantero et al., 2003) and the mPFC (Vijayan et al., 2017). Theta activity in the mPFC is associated with the processing and consolidation of emotional memories.

Our modeling work suggests that lower theta band activity may play a specific role in the suppression of fear memories. In particular, aspects of theta dynamics, such as the extent of external theta drive (from the hippocampus) in the human analog of IL, may determine the extent of REM-sleep-mediated fear extinction. Note that the human analog of IL is debated, but many researchers place it in the ventromedial prefrontal cortex (Laubach et al., 2018). Interestingly, human studies have implicated the ventromedial prefrontal cortex, along with the hippocampus, in fear extinction (Phelps et al., 2004; Milad et al., 2005, 2007; Kalisch, 2006).

Implications for PTSD

Individuals suffering from PTSD often repeatedly experience the same emotionally charged dream (Spoormaker and Montgomery, 2008) and show increased activity during REM sleep in limbic and cortical structures that regulate fear (Germain et al., 2013). We captured PTSD REM conditions by increasing NE levels during REM sleep in our model (Mellman et al., 1995). These conditions resulted in cells firing more irregularly and at higher frequencies and the dissipation of the theta rhythm. This result is in line with studies in PTSD patients suggesting that rhythmic activity is disrupted in frontal regions during REM sleep, although studies differ in their assessment of the exact nature of this change, with some suggesting reduction in frontal theta activity (Cowdin et al., 2014) and others suggesting increased power in higher frequencies (Wang et al., 2020) in the frontal cortex.

Under PTSD REM conditions, when 4 Hz theta activity was introduced to a cell assembly in IL (IL2, in our simulations), the synaptic changes that occurred did not result in a significant reduction in the activity of the associated fear memory in the amygdala (BA2 cell assembly). In other words, 4 Hz theta input to the IL, which may help to extinguish fear memories under normal REM sleep conditions, appears to be ineffective at doing so under PTSD REM conditions. Studies suggest that memories with a high emotional valence have a greater likelihood of being processed during sleep (Stickgold and Walker, 2013). Together, these factors could result in the same fearful dreams being

experienced over and over in PTSD patients. In other words, individuals with PTSD may not extinguish the fear associated with traumatic memories during REM sleep, whereas healthy individuals do. Whether fear extinction in healthy individuals occurs in one night of sleep or over multiple nights and multiple dreams, and whether the unconditioned stimulus is present in these dreams are very interesting questions that require further investigation. With respect to the first question, whether multiple nights are required might depend on the initial magnitude of the emotional charge of the fear memory and how much emotional charge is dissipated by a single dream.

Surprisingly, when 10 Hz activity was introduced to a cell assembly in IL (IL2, in our simulations), synaptic changes occurred in the same direction and to a similar extent as the changes that occurred when 4Hz theta frequency inputs were introduced under the physiological conditions of normal REM sleep; connections from IL to the amygdala (IL2 to BA) were strengthened, whereas those from the amygdala to IL (BA to IL2) were weakened. Furthermore, the firing rates of the cells representing the associated fear memory in the amygdala (BA2) were significantly reduced. This result suggests that neuromodulation of mPFC activity of ~10 Hz during REM sleep may have therapeutic value for ameliorating the symptoms of PTSD. There are various options for implementing such neuromodulation in practice. For instance, transcranial direct current stimulation (tDCS) during sleep has been shown to boost oscillatory activity and enhance learning (Marshall et al., 2006). Our work suggests that tDCS at 10 Hz over midline frontal areas during REM sleep might help extinguish fear memories in PTSD patients. Alternatively, tDCS at 4 Hz over midline frontal areas during REM sleep might help restore normal theta activity in these areas and thereby help extinguish fear memories in PTSD patients. Auditory stimulation during sleep has also been shown to enhance oscillations, especially during non-REM sleep. Recent work has shown that auditory stimulation may be effective in enhancing oscillatory activity in REM sleep as well (Harrington et al., 2021). Thus, there is potential to develop an auditory stimulation paradigm for the induction of 4 Hz or 10 Hz oscillations during REM sleep. Such a protocol may provide a means for therapeutic intervention in PTSD patients.

Our modeling results also provide insight into recent findings that show that in individuals with sleep disorders, REM sleep is related to poorer extinction of fear memories, whereas in healthy individuals REM sleep is related to better fear extinction (Bottary et al., 2020). In particular, our model shows how aberrations in REM sleep dynamics in the circuits responsible for emotional memory processing could render inputs that normally would help consolidate emotional memories ineffective or even produce changes in the opposite direction (e.g., increase fear associated with a memory rather than reduce it).

We also note that our modeling results coincide with the results of recent studies showing that sub-bands within the theta band are critical for communication within and between the mPFC and limbic structures and that neurotransmitters can enhance or impair communication within these structures in theta sub-bands. For instance, studies suggest that the coherence between the hippocampus and the mPFC of theta frequencies near the upper end of the theta range is important for avoidance learning (Padilla-Coreano et al., 2019; Dickson et al., 2022). Padilla-Coreano et al. (2019) found that oscillatory optogenetic stimulation of hippocampal terminals in the mPFC during an avoidance behavior task maximally increased avoidance when delivered at a frequency of 8 Hz rather than 2, 4, or 20 Hz. And

interestingly, Dickson et al. (2022) found that coherence in theta subfrequencies (in particular at \sim 6, 9, and 11 Hz) changed dynamically during the course of the avoidance response. Furthermore, Kjaerby et al. (2016) found that the effectiveness of theta band communication could be modulated by neurotransmitters. In particular, they showed that serotonin could act on terminals in the prefrontal cortex originating from the hippocampus and the contralateral prefrontal cortex to reduce both theta activity and avoidance behavior. Along the same lines, high norepinephrine levels in our model under otherwise healthy REM sleep conditions dissipate theta activity and reduce the ability of lower theta band activity (4 Hz) to suppress fear memories while at the same time making higher range (10 Hz) theta inputs to IL more effective in inducing plastic changes in IL–amygdala connections.

References

- Avesar D, Stephens EK, Gulledge AT (2018) Serotonergic regulation of corticoamygdalar neurons in the mouse prelimbic cortex. Front Neural Circuits 12:63.
- Bacon SJ, Headlam AJN, Gabbott PLA, Smith AD (1996) Amygdala input to medial prefrontal cortex (mPFC) in the rat: a light and electron microscope study. Brain Res 720:211–219.
- Baran B, Pace-Schott EF, Ericson C, Spencer RMC (2012) Processing of emotional reactivity and emotional memory over sleep. J Neurosci 32:1035– 1042
- Barth A, Vizi E, Lendvai BL (2007) Noradrenergic enhancement of Ca2+ responses of basal dendrites in layer 5 pyramidal neurons of the prefrontal cortex. Neurochem Int 51:323–327.
- Bazhenov M, Stopfer M, Rabinovich M, Huerta R, Abarbanel HDI, Sejnowski TJ, Laurent G (2001) Model of transient oscillatory synchronization in the locust antennal lobe. Neuron 30:553–567.
- Bi G, Poo M (1998) Synaptic modifications in cultured hippocampal neurons: dependence on spike timing, synaptic strength, and postsynaptic cell type. J Neurosci 18:10464–10472.
- Bloodgood DW, Sugam JA, Holmes A, Kash TL (2018) Fear extinction requires infralimbic cortex projections to the basolateral amygdala. Transl Psychiat 8:60.
- Bocchio M, Fucsina G, Oikonomidis L, McHugh SB, Bannerman DM, Sharp T, Capogna M (2015) Increased serotonin transporter expression reduces fear and recruitment of parvalbumin interneurons of the amygdala. Neuropsychopharmacology 40:3015–3026.
- Bocchio M, McHugh SB, Bannerman DM, Sharp T, Capogna M (2016) Serotonin, amygdala and fear: assembling the puzzle. Front Neural Circuit 10:24.
- Bottary RM, Seo J, Daffre C, Gazecki S, Moore KN, Kopotiyenko K, Dominguez JP, Gannon K, Lasko NB, Roth B, Milad MR, Pace-Schott EF (2020) Fear extinction memory is negatively associated with REM sleep in insomnia disorder. Sleep 43:
- Bouton ME, Westbrook RF, Corcoran KA, Maren S (2006) Contextual and temporal modulation of extinction: behavioral and biological mechanisms. Biol Psychiatry 60:352–360.
- Boyce R, Glasgow SD, Williams S, Adamantidis A (2016) Causal evidence for the role of REM sleep theta rhythm in contextual memory consolidation. Science 352:812–816.
- Burgos-Robles A, Vidal-Gonzalez I, Quirk GJ (2009) Sustained conditioned responses in prelimbic prefrontal neurons are correlated with fear expression and extinction failure. J Neurosci 29:8474–8482.
- Cairney SA, Durrant SJ, Power R, Lewis PA (2015) Complementary roles of slow-wave sleep and rapid eye movement sleep in emotional memory consolidation. Cereb Cortex 25:1565–1575.
- Cantero JL, Atienza M, Stickgold R, Kahana MJ, Madsen JR, Kocsis B (2003) Sleep-dependent theta oscillations in the human hippocampus and neocortex. J Neurosci Official J urosci 23:10897–10903.
- Carr DB, Andrews GD, Glen WB, Lavin A (2007) alpha2-Noradrenergic receptors activation enhances excitability and synaptic integration in rat prefrontal cortex pyramidal neurons via inhibition of HCN currents. J Physiol 584:437–450.

- Cowdin N, Kobayashi I, Mellman TA (2014) Theta frequency activity during rapid eye movement (REM) sleep is greater in people with resilience versus PTSD. Exp Brain Res 232:1479–1485.
- Datta S, O'Malley MW (2013) Fear extinction memory consolidation requires potentiation of pontine-wave activity during REM sleep. J Neurosci 33:4561–4569.
- Dickson CR, Holmes GL, Barry JM (2022) Dynamic θ frequency coordination within and between the prefrontal cortex–hippocampus circuit during learning of a spatial avoidance task. eNeuro 9:ENEURO.0414-21.2022.
- Durstewitz D, Seamans JK (2002) The computational role of dopamine D1 receptors in working memory. Neural Netw 15:561–572.
- Durstewitz D, Gabriel T (2007) Dynamical basis of irregular spiking in NMDA-driven prefrontal cortex neurons. Cereb Cortex 17:894–908.
- Durstewitz D, Seamans JK, Sejnowski TJ (2000) Dopamine-mediated stabilization of delay-period activity in a network model of prefrontal cortex. J Neurophysiol 83:1733–1750.
- Duvarci S, Pare D (2014) Amygdala microcircuits controlling learned fear. Neuron 82:966–980.
- Faber ESL, Callister RJ, Sah P (2001) Morphological and electrophysiological properties of principal neurons in the rat lateral amygdala in vitro. J Neurophysiol 85:714–723.
- Fu J, Li P, Ouyang X, Gu C, Song Z, Gao J, Han L, Feng S, Tian S, Hu B (2007) Rapid eye movement sleep deprivation selectively impairs recall of fear extinction in hippocampus-independent tasks in rats. Neuroscience 144:1186–1192.
- Germain A, James J, Insana S, Herringa RJ, Mammen O, Price J, Nofzinger E (2013) A window into the invisible wound of war: functional neuroimaging of REM sleep in returning combat veterans with PTSD. Psychiatry Res 211:176–179.
- Gerstner W, Kistler WM (2002) Mathematical formulations of Hebbian learning. Biol Cybern 87:404–415.
- Ghashghaei HT, Barbas H (2002) Pathways for emotion: interactions of prefrontal and anterior temporal pathways in the amygdala of the rhesus monkey. Neuroscience 115:1261–1279.
- Ghashghaei HT, Hilgetag CC, Barbas H (2007) Sequence of information processing for emotions based on the anatomic dialogue between prefrontal cortex and amygdala. Neuroimage 34:905–923.
- Gütig R, Aharonov R, Rotter S, Sompolinsky H (2003) Learning input correlations through nonlinear temporally asymmetric Hebbian plasticity. J Neurosci 23:3697–3714.
- Harrington MO, Ashton JE, Ngo H-VV, Cairney SA (2021) Phase-locked auditory stimulation of theta oscillations during rapid eye movement sleep. Sleep 44:zsaa227.
- Herry C, Ciocchi S, Senn V, Demmou L, Müller C, Lüthi A (2008) Switching on and off fear by distinct neuronal circuits. Nature 454:600–606.
- Hill S, Tononi G (2005) Modeling sleep and wakefulness in the thalamocortical system. J Neurophysiol 93:1671–1698.
- Ji X-H, Cao X-H, Zhang C-L, Feng Z-J, Zhang X-H, Ma L, Li B-M (2008) Pre- and postsynaptic -adrenergic activation enhances excitatory synaptic transmission in layer V/VI pyramidal neurons of the medial prefrontal cortex of rats. Cereb Cortex 18:1506–1520.
- Johnson LR, Hou M, Prager EM, LeDoux JE (2011) Regulation of the fear network by mediators of stress: norepinephrine alters the balance between cortical and subcortical afferent excitation of the lateral amygdala. Front Behav Neurosci 5:23.
- Jung MW, Qin Y, McNaughton BL, Barnes CA (1998) Firing characteristics of deep layer neurons in prefrontal cortex in rats performing spatial working memory tasks. Cereb Cortex 8:437–450.
- Kalisch R, Korenfeld E, Stephan KE, Weiskopf N, Seymour B, Dolan RJ (2006) Context-dependent human extinction memory is mediated by a ventromedial prefrontal and hippocampal network. J Neurosci 26:9503– 9511
- Kim D, Paré D, Nair SS (2013) Mechanisms contributing to the induction and storage of Pavlovian fear memories in the lateral amygdala. Learn Mem 20:421–430.
- Kim SY, Kark SM, Daley RT, Alger SE, Rebouças D, Kensinger EA, Payne JD (2020) Interactive effects of stress reactivity and rapid eye movement sleep theta activity on emotional memory formation. Hippocampus 30:829–841.

- Kjaerby C, Athilingam J, Robinson SE, Iafrati J, Sohal VS (2016) Serotonin 1B receptors regulate prefrontal function by gating callosal and hippocampal inputs. Cell Reports 17:2882–2890.
- Laubach M, Amarante LM, Swanson K, White SR (2018) What, if anything, is rodent prefrontal cortex? eNeuro 5:ENEURO.0315-18.2018.
- Li G, Nair SS, Quirk GJ (2009) A biologically realistic network model of acquisition and extinction of conditioned fear associations in lateral amygdala neurons. J Neurophysiol 101:1629–1646.
- Little JP, Carter AG (2013) Synaptic mechanisms underlying strong reciprocal connectivity between the medial prefrontal cortex and basolateral amygdala. J Neurosci 33:15333–15342.
- Maquet P, Péters J-M, Aerts J, Delfiore G, Degueldre C, Luxen A, Franck G (1996) Functional neuroanatomy of human rapid-eye-movement sleep and dreaming. Nature 383:163–166.
- Marshall L, Helgadóttir H, Mölle M, Born J (2006) Boosting slow oscillations during sleep potentiates memory. Nature 444:610–613.
- McCormick DA (1992) Neurotransmitter actions in the thalamus and cerebral cortex and their role in neuromodulation of thalamocortical activity. Prog Neurobiol 39:337–388.
- McGarry LM, Carter AG (2017) Prefrontal cortex drives distinct projection neurons in the basolateral amygdala. Cell Rep 21:1426–1433.
- Mellman TA, Kumar A, Kulick-Bell R, Kumar M, Nolan B (1995) Nocturnal/daytime urine noradrenergic measures and sleep in combat-related PTSD. Biol Psychiatry 38:174–179.
- Milad MR, Quirk GJ (2002) Neurons in medial prefrontal cortex signal memory for fear extinction. Nature 420:70–74.
- Milad MR, Quinn BT, Pitman RK, Orr SP, Fischl B, Rauch SL (2005) Thickness of ventromedial prefrontal cortex in humans is correlated with extinction memory. Proc Natl Acad Sci U S A 102:10706–10711.
- Milad MR, Wright CI, Orr SP, Pitman RK, Quirk GJ, Rauch SL (2007) Recall of fear extinction in humans activates the ventromedial prefrontal cortex and hippocampus in concert. Biol Psychiatry 62:446–454.
- Nishida M, Pearsall J, Buckner RL, Walker MP (2009) REM sleep, prefrontal theta, and the consolidation of human emotional memory. Cereb Cortex 19:1158–1166.
- Nofzinger EA, Mintun MA, Wiseman M, Kupfer DJ, Moore RY (1997) Forebrain activation in REM sleep: an FDG PET study. Brain Res 770:192–201.
- Onge JRS, Stopper CM, Zahm DS, Floresco SB (2012) Separate prefrontalsubcortical circuits mediate different components of risk-based decision making. J Neurosci 32:2886–2899.
- Pace-Schott EF, Verga PW, Bennett TS, Spencer RMC (2012) Sleep promotes consolidation and generalization of extinction learning in simulated exposure therapy for spider fear. J Psychiatr Res 46:1036–1044.
- Pace-Schott EF, Tracy LE, Rubin Z, Mollica AG, Ellenbogen JM, Bianchi MT, Milad MR, Pitman RK, Orr SP (2014) Interactions of time of day and sleep with between-session habituation and extinction memory in young adult males. Exp Brain Res 232:1443–1458.
- Padilla-Coreano N, Canetta S, Mikofsky RM, Alway E, Passecker J, Myroshnychenko MV, Garcia-Garcia AL, Warren R, Teboul E, Blackman DR, Morton MP, Hupalo S, Tye KM, Kellendonk C, Kupferschmidt DA, Gordon JA (2019) Hippocampal-prefrontal theta transmission regulates avoidance behavior. Neuron 104:601–610.e4.
- Pape H-C, Pare D (2010) Plastic synaptic networks of the amygdala for the acquisition, expression, and extinction of conditioned fear. Physiol Rev 90:419–463.
- Payne JD, Stickgold R, Swanberg K, Kensinger EA (2008) Sleep preferentially enhances memory for emotional components of scenes. Psychol Sci 19:781–788.
- Payne JD, Kensinger EA, Wamsley EJ, Spreng RN, Alger SE, Gibler K, Schacter DL, Stickgold R (2015) Napping and the selective consolidation of negative aspects of scenes. Emotion 15:176–186.
- Pendyam S, Bravo-Rivera C, Burgos-Robles A, Sotres-Bayon F, Quirk GJ, Nair SS (2013) Fear signaling in the prelimbic-amygdala circuit: a computational modeling and recording study. J Neurophysiol 110:844–861.
- Pfister J-P, Gerstner W (2006) Triplets of spikes in a model of spike timingdependent plasticity. J Neurosci 26:9673–9682.
- Phelps EA, Delgado MR, Nearing KI, LeDoux JE (2004) Extinction learning in humans role of the amygdala and vmPFC. Neuron 43:897–905.

- Popa D, Duvarci S, Popescu AT, Léna C, Paré D (2010) Coherent amygdalocortical theta promotes fear memory consolidation during paradoxical sleep. Proc Natl Acad Sci U S A 107:6516–6519.
- Quirk GJ, Repa JC, LeDoux JE (1995) Fear conditioning enhances short-latency auditory responses of lateral amygdala neurons: parallel recordings in the freely behaving rat. Neuron 15:1029–1039.
- Rasch B, Born J (2013) About sleep's role in memory. Physiol Rev 93:681–766.
 Rosenkranz JA, Grace AA (1999) Modulation of Basolateral Amygdala Neuronal
 Firing and Afferent Drive by Dopamine Receptor Activation In Vivo.
 J Neurosci 19:11027–11039.
- Sakurai Y, Osako Y, Tanisumi Y, Ishihara E, Hirokawa J, Manabe H (2018) Multiple approaches to the investigation of cell assembly in memory research—present and future. Frontiers Syst Neurosci 12:21.
- Seidenbecher T, Laxmi TR, Stork O, Pape H-C (2003) Amygdalar and hippocampal theta rhythm synchronization during fear memory retrieval. Science 301:846–850.
- Sherfey JS, Soplata AE, Ardid S, Roberts EA, Stanley DA, Pittman-Polletta BR, Kopell NJ (2018a) DynaSim: a MATLAB toolbox for neural modeling and simulation. Front Neuroinform 12:10.
- Sherfey JS, Ardid S, Hass J, Hasselmo ME, Kopell NJ (2018b) Flexible resonance in prefrontal networks with strong feedback inhibition. Plos Comput Biol 14:e1006357.
- Sierra-Mercado D, Padilla-Coreano N, Quirk GJ (2011) Dissociable roles of prelimbic and infralimbic cortices, ventral hippocampus, and basolateral amygdala in the expression and extinction of conditioned fear. Neuropsychopharmacology 36:529–538.
- Song C, Moyer JR (2018) Layer- and subregion-specific differences in the neurophysiological properties of rat medial prefrontal cortex pyramidal neurons. J Neurophysiol 119:177–191.
- Sotres-Bayon F, Quirk GJ (2010) Prefrontal control of fear: more than just extinction. Curr Opin Neurobiol 20:231–235.
- Spoormaker VI, Montgomery P (2008) Disturbed sleep in post-traumatic stress disorder: secondary symptom or core feature? Sleep Med Rev 12:169–184.
- Spoormaker VI, Sturm A, Andrade KC, Schröter MS, Goya-Maldonado R, Holsboer F, Wetter TC, Sämann PG, Czisch M (2010) The neural correlates and temporal sequence of the relationship between shock exposure, disturbed sleep and impaired consolidation of fear extinction. J Psychiatr Res 44:1121–1128.
- Spoormaker VI, Schröter MS, Andrade KC, Dresler M, Kiem SA, Goya-Maldonado R, Wetter TC, Holsboer F, Sämann PG, Czisch M (2012) Effects of rapid eye movement sleep deprivation on fear extinction recall and prediction error signaling. Hum Brain Mapp 33:2362–2376.
- Stickgold R, Walker MP (2013) Sleep-dependent memory triage: evolving generalization through selective processing. Nat Neurosci 16:139–145.
- Uhlenbeck GE, Ornstein LS (1930) On the theory of the Brownian motion. Phys Rev 36:823–841.
- Vijayan S, Kopell NJ (2012) Thalamic model of awake alpha oscillations and implications for stimulus processing. Proc Natl Acad Sci U S A 109:18553–18558.
- Vijayan S, Lepage KQ, Kopell NJ, Cash SS (2017) Frontal beta-theta network during REM sleep. Elife 6:e18894.
- Wagner U, Gais S, Born J (2001) Emotional memory formation is enhanced across sleep intervals with high amounts of rapid eye movement sleep. Learn Mem 8:112–119.
- Wagner U, Hallschmid M, Rasch B, Born J (2006) Brief sleep after learning keeps emotional memories alive for years. Biol Psychiatry 60:788–790.
- Wang C, Ramakrishnan S, Laxminarayan S, Dovzhenok A, Cashmere JD, Germain A, Reifman J (2020) An attempt to identify reproducible highdensity EEG markers of PTSD during sleep. Sleep 43:
- Washburn M, Moises H (1992) Electrophysiological and morphological properties of rat basolateral amygdaloid neurons *in vitro*. J Neurosci 12:4066–4079.
- Watson BO, Levenstein D, Greene JP, Gelinas JN, Buzsáki G (2016) Network Homeostasis and State Dynamics of Neocortical Sleep. Neuron 90:839–852.
- Wolff SBE, Gründemann J, Tovote P, Krabbe S, Jacobson GA, Müller C, Herry C, Ehrlich I, Friedrich RW, Letzkus JJ, Lüthi A (2014) Amygdala interneuron subtypes control fear learning through disinhibition. Nature 509:453–458.
- Yizhar O, Klavir O (2018) Reciprocal amygdala-prefrontal interactions in learning. Curr Opin Neurobiol 52:149–155.